Nanoscale

Accepted Manuscript

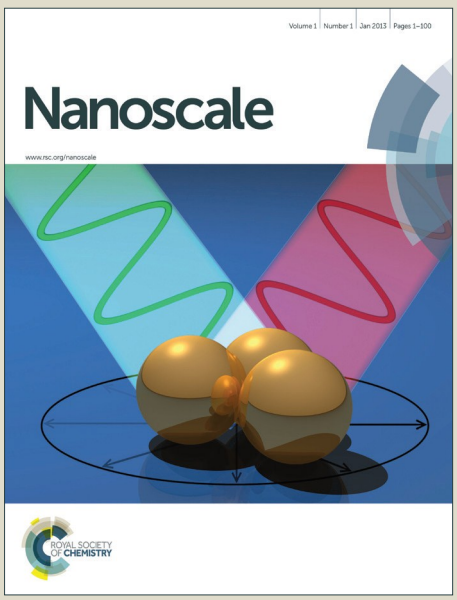

ROYAL SOCIETY OF CHEMISTRY

www.rsc.org/nanoscale

Does P-type Ohmic Contact Exist in WSe_2-metal Interfaces?

Yangyang Wang,[1, 3,†] Ruo Xi Yang,[1,4,†] Ruge Quhe,[1,5,6,†] Hongxia Zhong,[1,7,†] Linxiao Cong,[1] Meng Ye,[1] Zeyuan Ni,[1] Zhigang Song,[1] Jinbo Yang,[1,2] Junjie Shi,[1] Ju Li,[3] and Jing Lu[1,2,*]

[1] State Key Laboratory for Mesoscopic Physics and Department of Physics, Peking University, Beijing 100871, P. R. China

[2] Collaborative Innovation Center of Quantum Matter, Beijing 100871, P. R. China

[3] Department of Nuclear Science and Engineering and Department of Materials Science and Engineering, Massachusetts Institute of Technology, Cambridge, Massachusetts 02139 , USA

[4] Department of Chemistry, University of Bath, Claverton Down, Bath BA2 7AY, UK

[5] State Key Laboratory of Information Photonics and Optical Communications & School of Science, Beijing University of Posts and Telecommunications, Beijing 100876, China

[6] Academy for Advanced Interdisciplinary Studies, Peking University, Beijing 100871, China

[7] Department of Physics, Washington University in St. Louis, St. Louis, Missouri 63130, USA

[†]These authors contributed equally to this work.

[*]Address correspondence to: jinglu@pku.edu.cn

ABSTRACT

Formation of low-resistance metal contacts is the biggest challenge that masks the intrinsic exceptional electronic properties of two dimensional WSe_2 devices. We present the first comparative study of the interfacial properties between monolayer/bilayer (ML/BL) WSe_2 and Sc, Al, Ag, Au, Pd, and Pt contacts by using *ab initio* energy band calculations with inclusion of the spin-orbital coupling (SOC) effects and quantum transport simulations. The interlayer coupling tends to reduce both the electron and hole Schottky barrier heights (SBHs) and alters the polarity for WSe_2-Au contact, while the SOC chiefly reduces the hole SBH. In the absence of the SOC, Pd contact has the smallest hole SBH. Dramatically, Pt contact surpasses Pd contact and becomes *p*-type Ohmic or quasi-Ohmic contact with inclusion of the SOC. Therefore, *p*-type Ohmic or quasi-Ohmic contact exists in WSe_2-metal interfaces. Our study provides a theoretical foundation for the selection of favorable metal electrodes in ML/BL WSe_2 devices.

Keywords: WSe_2, Interface, Schottky barrier, Density functional theory, Quantum transport simulation

Introduction

Two dimensional (2D) transition-metal dichalcogenides (TMDs) are attracting much recent attention because they have a wide range of application prospects in electronics,[1-7] photoelectronics,[1, 8-11] spintronics,[12-14] and valleytronics.[13, 15-20] Among 2D TMDs, monolayer (ML) and bilayer (BL) MoS_2 and WSe_2 are probably most intensively studied. 2D WSe_2 distinguishes it from 2D MoS_2 mainly in two aspects: (1) 2D WSe_2 has a much enhanced spin-orbit coupling (SOC) due to heavier W and Se atoms.[13, 14] For example, the splitting of the valence band maximum (VBM) is about 0.15 eV in ML MoS_2 but is enhanced to 0.46 eV in ML WSe_2.[13] Therefore, 2D WSe_2 is more suitable for spintronics purpose. (2) 2D MoS_2 favors *n*-type doping,[2, 3, 21] whereas 2D WSe_2 prefers *p*-type doping as a result of much higher positions of the conduction band minimum (CBM) and the VBM.[5, 6, 22] A *p*-*n* junction can be fabricated with 2D MoS_2 as *n* region and 2D WSe_2 as *p* region, and such a device has been reported recently, with excellent rectification behavior and rapid photoresponse.[18, 23]

A device often needs a contact with metal electrodes, and the formation of low-resistance metal contacts is the biggest challenge that masks the intrinsic exceptional electronic properties of 2D TMDs.[21] In the absence of a controllable and sustainable substitutional doping scheme, one has to rely on the work function of contact metals to inject appropriate types of carriers into the respective bands of 2D TMDs. Such metal-semiconductor contacts are often associated with a formation of finite Schottky barrier, which decreases the carrier injection efficiency. Apparently, decreasing Schottky barrier height (SBH) is critical to reach a high performance of a device, and a low resistance Ohmic contact with vanishing SBH is highly desirable. Unfortunately, the SBH does not simply depend on the difference between the intrinsic Fermi level (E_f) of a metal and the CBM or VBM of the semiconductor due to the complex Fermi level pinning, which renders the appearance of Ohmic contact rather difficult.[24, 25]

There have been a lot of works to study 2D MoS_2-metal interfaces.[21, 26-31] However, in terms of the recent reports the Fermi level of elemental metals is pinned close to the conduction band of MoS_2, and no *n*-type low-resistance Ohmic contact has been revealed either experimentally or theoretically in 2D MoS_2 even with low work function metals such as Ti and Sc.[3, 21, 24, 32] Inserting a monolayer *h*-BN can break the interface interaction between metal and MoS_2, thus efficiently lowering the Fermi level pinning and attain vanishing *n*-type SBHs based on the density functional calculations.[33] Ni-etched graphene has been proved experimentally as an effective buffer layer to reduce the *n*-type contact resistance of MoS_2-Ni.[34] To achieve efficient hole contacts experimentally, molybdenum trioxide (MoO_x, $x<3$)[35, 36] is used as a buffer layer between metal and MoS_2 and show unambiguous advantages of hole injections over the conventionally explored metal contacts, mainly

due to their high work functions and relatively weak Fermi level pinning at the interfaces. The utilization of graphene oxide[37] was also proposed and demonstrated as a promising hole injection layer by using first-principles computations.

Compared with those about MoS_2, the studies of 2D WSe_2-metal interfaces are much limited. In the experimental aspect, Javey *et al.*'s measurement showed that high work function Pd forms the lowest resistance to the valence band of ML WSe_2 for hole transport, while lower function Ag, Ni, Au, Ti, and Gd have high SBH to both the valence band and the conduction band of ML WSe_2.[5] Banerjee *et al*. claimed that Al forms a *n*-type Schottky contact with ML WSe_2, but Ti, In, and Ag form *n*-type Ohmic contacts according to their measured output linear characteristics.[4] In the theoretical aspect, Schottky barrier is always present in ML WSe_2 and In, Ti, Al, Au, and Pd interfaces, where the SOC is not considered in the energy band calculations.[4, 21] Three fundamental issues arise: (1) Which elemental metal has the smallest hole SBH when contacted with WSe_2? (2) Whether *p*-type Ohmic contact is present in ML WSe_2-metal contacts? (3) What are the effects of the SOC on the SBH of ML WSe_2-metal contacts? The SBH depends on the difference between E_f of the metal electrode and the band edge of the channel semiconductor in a device environment. Given a rise of 0.23 eV of the VBM due to the SOC splitting in ML WSe_2,[13] the ignorance of it in determining the hole SBH appears rather unacceptable unless existence of a full Fermi level pining during the SOC process.

Due to the strong interlayer coupling, BL WSe_2 has a reduced band gap compared with ML one (1.44 eV vs 1.67 eV at the density functional theory (DFT) level).[38] Therefore, a reduced SBH and thus a higher carrier injection efficiency can be expected in BL WSe_2-metal contacts, suggesting a better device performance of BL WSe_2 as the channel compared with ML WSe_2 given an identical gate voltage controllability. However, to the best of our knowledge, the interfacial properties of BL WSe_2-metal contacts have not been investigated.

In this Article, we provide a comparative study of the interfacial properties of ML and BL WSe_2 on several commonly used metals (Sc, Al, Ag, Au, Pd, and Pt), for the first time by using the DFT energy band calculation with inclusion of the SOC effects. We find that the interlayer coupling decreases both the electron and hole SBHs and even alters the polarity of WSe_2-Au contact. No Ohmic contact is revealed in the absence of the SOC, and Pd contact has the minimum hole SBH (0.22/0.27 eV for ML/BL WSe_2 case). However, when the SOC is included, ML and BL WSe_2-Pt interfaces dramatically have the minimum hole SBHs and actually become *p*-type Ohmic or quasi-Ohmic contact. A more reliable approach to treat the SBH is *ab initio* quantum transport

simulation based on a two-probe model, which is also performed and gives a hole SBH similar to that of the energy band calculation for ML WSe_2-Pt interface in the absence of the SOC.

Computational methods

The geometry optimizations are carried out by employing the CASTEP package[39] with the ultrasoft pseudopotential[40] and plane-wave basis set. The cut-off energy is 400 eV. To take the dispersion interaction into account, a DFT-D semiempirical dispersion-correction approach is used with the Ortmann-Bechstedt-Schmidt (OBS) scheme.[41] The dipole correction to the total energies is adopted. The stopping criteria for the ionic relaxation are such that the remnant force on each atom is below 0.01 eV/Å and that energies are converged to within 10^{-5} eV per atom. The electronic structures are calculated with the projector-augmented wave (PAW) pseudopotential[42, 43] and plane-wave basis set with a cut-off energy of 400 eV implemented in the Vienna *ab initio* simulation package (VASP) in order to analyze the band components.[44-47] The Monkhorst-Pack[48] *k*-point mesh is sampled with a separation of about 0.10 and 0.03 $Å^{-1}$ in the Brillouin zone during the relaxation and electronic calculation periods, respectively. Our tests show that the band structures generated from CASTEP and VASP packages coincide well.

The WSe_2 transistor is simulated using the DFT coupled with the nonequilibrium Green's function (NEGF) method, as implemented in the ATK 11.8 package [46, 47]. The single-zeta plus polarization (SZP) basis set is used. The Monkhorst-Pack *k*-point meshes for the central region and electrodes are sampled with 1×50×1 and 50×50×1 separately. The temperature is set to 300 K. The Neumann condition is used on the boundaries of the direction vertical to the WSe_2 plane. On the surfaces connecting the electrodes and the central region, we employ Dirichlet boundary condition to ensure the charge neutrality in the source and the drain region. The transmission coefficient at energy E averaged over 50 k_y-points perpendicular to the transport direction (x direction) is obtain by

$$T(E) = \mathrm{Tr}[G^r \Gamma_L(E) G^a \Gamma_R(E)] \quad (1)$$

Where $G^{r(a)}$ is the retarded (advanced) Green function and $\Gamma_{L(R)}(E) = i(\Sigma^r_{L(R)} - \Sigma^a_{L(R)})$ is the level broadening due to left (right) electrode expressed in terms of the electrode self-energy $\Sigma_{L(R)}$. Throughout the paper, the generalized gradient approximation (GGA) functional to the exchange-correction functional of the Perdew–Wang 91 (PW91) form[49] is adopted.

Results and discussion

Interface modeling and stability

We use six layers of metal atoms (Sc in (0001) orientation and Al, Ag, Au, Pd and Pt in (111) orientation) to model the metal surface because 6-layer metal atoms can give converged properties of the contact system according to the convergence tests done in the previous studies[21, 27] and ours. The calculated in-plane lattice constant of WSe_2 is a = 3.29 Å, in good agreement with the experimental value.[50] As the properties of WSe_2 are sensitive to its lattice parameter, we fix the lattice constant of WSe_2 to its optimized value and adjust the metal lattice to be commensurable to the WSe_2 lattice. The (1 × 1) unit cell of Sc (0001) face is adjusted to the (1 × 1) unit cell of WSe_2, and (2 × 2) unit cells of Al, Ag, Au, Pd and Pt (111) faces are adjusted to the ($\sqrt{3} \times \sqrt{3}$) R30° unit cell of WSe_2. The lattice mismatch in each metal is listed in the Table 1, ranging from 0.91%~3.19%. The in-plane lattice constant of the supercell is fixed during the relaxation. A vacuum buffer space of at least 20 Å is set to avoid spurious interaction between periodic images. The most stable ML WSe_2-metal contact geometries are obtained by optimizing the structures from different initial configurations. The initial configurations of BL WSe_2-metal interfaces are constructed in terms of AA′ stacking in WSe_2 (a D_{3d} point group symmetry)[51] on the basis of the most stable ML WSe_2-metal interface configurations.

The most stable configurations of the ML WSe_2-metal interfaces are shown in Figure 1. The relative positions between ML WSe_2 and metal substrates along the interface directions are different for different metals. On Sc(0001) surface, the W atoms in the primitive cell sit above the top metal atoms, and the Se atoms sit above the second layer metal atoms (Figure 1c); On Al and Pt (111) surfaces, the W atoms in the supercell are all above the centers of the triangles formed by the fcc, hcp, and top sites, and the three pairs of Se atoms sit above the fcc, hcp, and top sites, respectively (Figure 1d); On Pd (111), the three W atoms in the supercell sit above the fcc, hcp, and top sites, respectively, and the Se atoms are all above the centers of the triangles formed by the fcc, hcp, and top sites (Figure 1e); On Ag and Au(111), the W and Se atoms are all above the centers of the triangles formed by the fcc, hcp, and top sites (Figure 1f). The most stable configurations of the BL WSe_2-metal interfaces are similar with the corresponding ML ones. The equilibrium interfacial distances d_z in ML and BL WSe_2-metal contacts are insensitive to the WSe_2 layer number, varying from 2.271-2.959 Å (Table 1). The binding energy per interfacial W atom is defined as

$$E_b = (E_{WSe_2} + E_{metal} - E_{WSe_2\text{-}metal})/N_W \quad (2)$$

Where E_{WSe_2}, E_{metal}, and $E_{WSe_2\text{-}metal}$ are the relaxed energies for WSe_2, metal surface, and the combined system per supercell, respectively, and N_W is the number of interface W atoms per supercell. E_b ranges from 0.160 to 1.049 eV as listed in Table 1. Similar to the cases of MoS_2,[21] the

adsorption of ML and BL WSe_2-metal surfaces can be classified into weak bonding (Al, Ag and Au contacts) with E_b = 0.160-0.367 eV, medium bonding (Pt and Pd) with E_b = 0.525-0.706 eV, and strong bonding (Sc) with E_b = 0.918 (ML) and 1.049 (BL) eV according to the binding strength.

It is important to note that the Schottky barrier may form at two possible interfaces in a transistor as shown in Figure 1g: if the interaction between WSe_2 and the metal surface is weak, it forms at the source/drain interface (B) between the contacted WSe_2 and the metal surface in the vertical direction; otherwise, if the interaction between WSe_2 and the metal surface is strong, it forms at the source/drain-channel (D) interface between the contacted WSe_2 and channel WSe_2 in the lateral direction. Such a dual interface model has been employed in the recent MoS_2-, graphdiyne-, and ML phosphorene-metal contact studies.[21, 24, 25, 52] Compared with a single vertical interface model, which predicts an Ohmic contact between ML MoS_2 and Ti due to the strong band hybridization,[29] the dual interface model predicts a Schottky contact with an electron SBH of 0.22-0.35 eV.[21, 24] A significant electron SBH of 0.30-0.35 eV between ML MoS_2 and Ti is found experimentally,[21] justifying the dual interface model. Actually, the calculated (0.096 eV) and observed (0.065 eV) electron SBH for BL MoS_2-Ti[24, 53] based on the dual interface model also show a good consistency.

Because SBH depends on the band edge positions of the semiconductor, the band edge positions of the semiconductor must be accurately determined. The DFT-GGA is a single electron theory and indeed underestimates the band gap of an intrinsic semiconductor, where many-body effects are nonnegligible. The band gap and the CBM and VBM of an intrinsic semiconductor should be calculated by many-body Green's function approach within the GW approximation. However, in a FET configuration, the semiconductor is either doped by metal electrode or by gate, and in this case, electron-electron interaction is greatly screened by doped carriers, and single electron theory becomes a good approximation to the quasi-particle band gap and the band edge positions.[24, 26, 54] Take ML phosphorene as an example, the transport gap, quasi-particle band gap, optical gap, DFT-HSE (Heyd−Scuseria−Ernzerhof) band gap, and DFT-GGA band gap are 1.0,[55] 2.0~2.2,[56, 57] 1.3~1.53,[57, 58] 1.0~1.6,[59-61] and 0.91 eV, respectively. The DFT-GGA band gap is a good approximation for the transport gap. This point is also proved by a comparison between the calculated and observed SBHs in 2D MoS_2 devices. The experimentally extracted SBHs of ML and BL MoS_2-Ti contact are 0.30 ~ 0.35[21] and 0.065 eV[53], respectively, which are in agreement with the calculated values of 0.216 and 0.096 eV at the DFT-GGA level.[24] Hence, the transport gap and the CBM and VBM of a semiconductor in a FET configuration can be approximately described by

DFT-GGA, while the hybrid functional method and quasi-particle method tend to overestimate the transport gap.

SBHs and interface states

The band structures of ML WSe_2 and the combined systems are shown in Figure 2. The ML WSe_2 has a band gap of 1.60 eV when the SOC is absent, consistent with the reported DFT value of 1.67 eV.[38] Both the valence and conduction bands of ML WSe_2 are strongly destroyed when contacted with Sc, resulting in an absent vertical Schottky barrier for ML WSe_2-Sc contact. The majority of the ML WSe_2 bands are still identifiable when contacted with Al, Ag and Au surfaces because the weak interaction. When contacted with Pt and Pd surfaces, the valence bands of ML WSe_2 are hybridized slightly with the *d*-bands of Pt and Pd, while the conduction bands are preserved well. Vertical Schottky barrier $\Phi_V^{e/h}$ for these weak or medium bonding cases (Figure 1g) can be obtained from the energy difference between E_f of the interfacial system and the CBM (electron SBH) or VBM (hole SBH) of the contacted WSe_2. Strictly speaking, the terminology band is appropriate for homogeneous crystals, whereas for heterogeneous interfaces with orbital hybridization, the CBM/VBM of the semiconductor side can be identified by regarding the spilled hybridization states as interfacial gap states.[26] As shown in Figure 2, the WSe_2 bands across the Fermi level with smaller weights originate from the band hybridization between WSe_2 and metals. They can be regards as a part of the interfacial gap states and won't affect the SBH. Therefore, the band gap and CBM/VBM of WSe_2 are determined through the projected WSe_2 states at the Γ point in the weak or medium bonding contacts. The band gap of ML WSe_2 becomes 1.57, 1.62, 1.56, 1.15 and 1.51 eV in the ML WSe_2-Al, -Ag, -Au, -Pd and -Pt contacts, respectively, which are generally smaller than that (1.60 eV) of the pristine WSe_2 because of the broadening of the energy bands induced by the perturbation of metal electrodes. In ML WSe_2-Al, -Ag and -Au contacts, as shown in Figure 2, the vertical Schottky barriers are *n*-type with electron SBH of Φ_V^e = 0.70, 0.50, and 0.66 eV, respectively. While in ML WSe_2-Pd and -Pt contacts, the vertical Schottky barriers are *p*-type with hole SBH of Φ_V^h = 0.22 and 0.34 eV, respectively. The vertical electron/hole SBH in ML WSe_2-Au/-Pd contact (0.66/0.22 eV) is comparable with the one (0.70/0.35 eV) calculated by Banerjee *et al.*[21] in the absence of the SOC effects. The nearly midgap SBH character of Al contact (Φ_V^e = 0.70 eV and Φ_V^h = 0.87 eV) is also consistent with the partial density of states (PDOS) calculations of Banerjee *et al.*.[4]

The band hybridization degree of the ML WSe_2-metal interfaces increases with the binding strength. The different bonding strength and band hybridization degree in different interfaces can be well explained by the *d*-band model.[62] Al has no *d*-orbitals and Ag and Au have full *d*-shells and they all bond with ML WSe_2 weakly, whereas Pt and Sc have open *d*-shells and bond with ML WSe_2 strongly. The relative position of *d*-band also plays an important role. As moving from the right to the left in the periodic table, the *d*-band moves up in energy. Although Pd and Ag both have full 4*d*-shells, the *d*-band of Pd is located nearer to E_f than that of Ag thus strongly hybridizes with the valence bands of WSe_2. The *d*-band of Sc is located near the conduction bands of ML WSe_2 in energy. Therefore, the conduction bands of ML WSe_2 are perturbed more seriously than its valence bands when contacted with Sc. Although the metal and W in WSe_2 are separated by a Se layer, their *d*-bands strongly hybridize with each other. Take ML WSe_2-Pt contact as an example, as shown in Figure S1a, we can find a clear hybridization between Pt and W *d*-bands as their *d*-band dispersion curves coincide with each other in some regions. The PDOS analysis shown in Figure S1b further confirms this point as there is a big bump around −1.2 eV for both the Pt and W *d*-orbitals.

To further study the contact natures in the vertical direction, the PDOS of W and Se atoms in ML WSe_2-metal contacts are provided in Figure 3. After contacted with metal faces, there appear electronic states in the original band gap of ML WSe_2. The PDOSs at E_f ($N(E_f)$) increases in this order: Au (0.39) < Al (0.50) < Ag (0.58) < Pt (1.08) < Pd (1.24) < Sc (2.1), a result consistent with the hybridization degree (for Sc contact, we compare its $3N(E_f)$ value with the $N(E_f)$ of other metal contacts because its interface unit cell area is 1/3 of others). The prominent overlap between Sc and WSe_2 in the original band gap of WSe_2 indicates a covalent bond formation between them, thus further confirming the absence of vertical Schottky barrier. In contrast, there are much fewer overlap interface states distributed in the original band gap for other contacts compared with those in the Sc contact. The overlap states near E_f not only play an important role in the Fermi level pinning,[26] also contribute to the electron or hole injections from the metal to the semiconductor in terms of the mechanism proposed by Heine[63] that the nature of these interface states origins from a decaying metallic wave function into the nanometer depth of semiconductors. Therefore, the PDOS value at E_f to a degree can reflect the quality of vertical contacts. For example, the PDOS near E_f in the ML WSe_2-Sc contact is rather large, and the vertical SBH vanishes in this contact.

The electronic structures of free-standing BL WSe_2 and BL WSe_2-metal interfaces are shown in Figure 4, with a smaller indirect band gap of 1.43 eV for free-standing BL WSe_2. The band hybridization degree is similar to ML and can also be divided into the same three categories. The

vertical Schottky barrier in BL WSe_2-Sc system is also absent due to the strong hybridization between the bands of BL WSe_2 and Sc. The band gap of BL WSe_2 becomes 1.12, 1.12, 1.43, 1.19 and 1.25 eV in the BL WSe_2-Al, -Ag, -Au, -Pd and -Pt contacts, respectively, which are also generally smaller than the value of the pristine one. In BL WSe_2-Al, -Ag, -Pd and -Pt contacts, the type of the vertical Schottky barrier is same as the ML case; the Schottky barriers are *n*-type with Φ_V^e = 0.37 and 0.30 eV in BL WSe_2-Al and -Ag, and are *p*-type with Φ_V^h = 0.27 and 0.32 eV in BL WSe_2-Pd and -Pt, respectively. In these four metal contacts, Φ_V^e is decreased significantly in the *n*-type contacts while Φ_V^h is not altered much in the *p*-type contacts compared with those in the cases of ML. The vertical Schottky barrier changes from weak *n*-type in ML WSe_2-Au contact to weak *p*-type with Φ_V^h = 0.58 eV in BL case. In both cases, E_f is close to the band gap center of WSe_2. Experimentally, ambipolarity is observed in few layer WSe_2 FET with Au electrode, a result consistent with our calculation.[64]

WSe_2 hosts heavy 5*d* elements with strong atomic SOC, much stronger than that in the more intensively studied MoS_2 system.[13] After inclusion of the SOC effects, the band structures of ML and BL WSe_2 are greatly modified as shown in the first and second panels of Figure 2 and 4 by lining up the bands with the vacuum level. The band gap of ML (BL) WSe_2 is reduced from 1.60(1.43) to 1.33(1.15) eV. The CBM of ML (BL) WSe_2 is changed slightly and only falls by 0.04 (-0.09) eV, but the VBM is significantly elevated by 0.23 (0.37) eV, after the SOC effects are included. Therefore, if the Fermi level pinning is absent during the SOC process, the electron vertical SBH is little affected, but the hole vertical SBH is decreased remarkably by about 0.23 (0.37) eV for ML (BL) case once the SOC effects are included. As shown in Figure 5, the CBMs of ML and BL WSe_2 is little changed (within 0.07 eV) in the Pd and Pt contacts. By contrast, the VBM of ML (BL) WSe_2 is lifted by 0.04 (0.18) eV in ML (BL) WSe_2-Pd contact after inclusion of the SOC effect, and thus we have a reduced Φ_V^h = 0.18 (0.09) eV for hole injection. The VBM in ML (BL) WSe_2-Pd contact is not elevated as high as in free-standing ML (BL) WSe_2, reflecting a partial Fermi level pining during the SOC process. The reduction in Φ_V^h is especially remarkable in Pt contact. The VBM of WSe_2 touches E_f in ML and BL WSe_2-Pt contacts after inclusion of the SOC effects because of the significant rise of the VBM by about 0.34 and 0.32 eV, respectively, leading to Ohmic or quasi-Ohmic interfaces. The rise amplitudes of the VBM in ML and BL WSe_2-Pt contacts are comparable with those in free-standing ML and BL WSe_2, implying a much depressed or even vanishing Fermi level pining during the SOC process in Pt contact. The predicted *p*-type Ohmic or quasi-Ohmic contact for ML and BL WSe_2-Pt is in agreement with the very recent experimental

results of Banerjee *et al.* that a dual-gated WSe_2 FET with Pt contacts has linear output characteristics in the low-voltage regime for all negative top biases even down to cryogenic temperature.[65] This indicates the importance of the SOC in determining the interfacial properties of 2D WSe_2-metal contacts. We note that the band gaps of ML (BL) WSe_2 become 1.04 (1.07) and 1.10 (0.87) eV in the Pd and Pt contacts, respectively, which remain smaller than the value in pristine WSe_2 of 1.33 (1.15) eV.

Because of the covalent bonding between WSe_2 and Sc, ML (BL) WSe_2-Sc can be regarded as a new metallic material. A lateral Schottky barrier is possibly formed at the interface D, and its height $\Phi_{\mathrm{L}}^{\mathrm{e/h}}$ is determined by the energy difference between E_f of the WSe_2-Sc complex system and the CBM (electron SBH) or VBM (hole SBH) of channel WSe_2. As has been discussed above, the transport gap of 2D TMD channel could be determined by the DFT band gap rather than the quasi-particle band gap or HSE band gap. As shown in Figure S2, lateral *n*-type Schottky barriers are formed for ML and BL WSe_2-Sc contacts with electron SBHs $\Phi_{\mathrm{L}}^{\mathrm{e(Non\text{-}SOC)}}$ = 0.29 and 0.16 eV and $\Phi_{\mathrm{L}}^{\mathrm{e(SOC)}}$ = 0.25 and 0.25 eV, respectively.

Fermi level pinning

The partial Fermi level pinning is a synergic result of the metal work function modification and the interface states formation in the studied interface systems.[26] Fermi level pinning makes the contact nature complex and difficult to predict. The absolute band alignments between pristine ML/BL WSe_2 and metals are offered in Figure S3. The differences between metal work functions and the CBM (VBM) of ML and BL WSe_2 are compared with the electron (hole) SBHs obtained by the energy band analysis of the interfacial systems in Figures S3b and S3d, respectively. The discrepancy in the values shows that there exists Fermi level pinning effect in the WSe_2-metal contacts. We define the Fermi energy shift ΔE_f as

$$\Delta E_f = \begin{cases} E_{\mathrm{D}} - E_f, \text{ for vertical Schottky barrier} \\ W - W_{\mathrm{WSe_2}}, \text{ for lateral Schottky barrier} \end{cases} \quad (3)$$

where E_{D} is the middle energy of the band gap of the WSe_2 adsorbed on metal substrates, E_f is the Fermi level of the interfacial system, W and $W_{\mathrm{WSe_2}}$ are the work functions of the combined system and pristine ML or BL WSe_2, respectively. Negative (positive) ΔE_f means *n*-type (*p*-type) doping of WSe_2. ΔE_f as a function of the difference between the clean metal and ML (BL) WSe_2 work functions $W_{\mathrm{M}} - W_{\mathrm{WSe_2}}$ is shown in Figure S4. We applying a linear fit to all the data obtained with or without the SOC effects. The slope is 0.40 in both ML and BL WSe_2-metal contacts, which is much smaller than the previously reported theoretical value of 0.64~0.71 in ML and BL MoS_2-metal

contacts,[24, 26] indicating a higher degree of interface Fermi-level pinning in the WSe_2 contacts. The slope close to 1 means no Fermi level pinning and close to 0 indicates a strong Fermi level pinning. We therefore observe a partial Fermi level pinning picture in the six ML (BL) WSe_2-metals contacts.

Tunneling barrier

The tunneling barrier is another figure of merit to evaluate a contact, here its height ΔV defined as the potential energy above E_f between the WSe_2 and metal surfaces,[66, 67] indicated by the black rectangular in Figure 6, and its width w_B defined as the full width at half maximum of the ΔV. In some metal contacts studies,[21, 29] the barrier height is defined as the difference between the potential energy at the top metal layer and the maximum of the potential between the interfaces. The barrier height in our definition presents the lowest barrier that the electrons at E_f need to overcome when injected from metal to TMDs, while in another definition,[19, 26] the barrier height means the highest barrier that the electrons need to overcome for injection. From a physical point of view, our definition more makes sense. As shown in Figure 6 and Table 2, the weak bonding (Al, Ag and Au) and medium bonding (Pd and Pt) interfaces have a notably high ΔV and a notably wide w_B. On the contrary, there is no tunneling barrier at the strong bonding interfaces (Sc), indicating a higher electron injection efficiency and thus a lower contact resistance. We estimate the tunneling probabilities T_B from metal to WSe_2 using a square potential barrier model as:

$$T_B = \exp(-2 \times \frac{\sqrt{2m\Delta V}}{\hbar} \times \omega_B) \quad (4)$$

where m is the effective mass of a free electron and $\hbar$ is the Plank's constant. The T_B values are thus estimated to be 100 (100), 26.9 (47.9), 39.9 (52.2), 34.3 (42.7), 52.4 (78.8) and 31.0 (41.0)% for ML (BL) WSe_2-Sc, Al, Ag, Au, Pd and Pt contacts, respectively. The tunneling probability is generally larger in the BL contact cases than the corresponding ML one. Apparently, Sc contacts have a perfect tunneling transmission. As discussed before, the PDOS value near E_f to a degree can reflect the quality of vertical contacts. The ML WSe_2-Pt, -Pd and -Sc contacts have larger PDOS values near E_f. Consistently, the tunneling probabilities in them are generally larger than those in other metal contacts.

Quantum transport simulation

A more direct and reliable approach to determine the SBH of a 2D WSe_2 transistor is the *ab initio* quantum transport simulation. As an example, in Figure 7, we present the simulated transport properties of ML WSe_2 transistor with Pt electrodes (the SOC is not included). The length of the channel is 73 Å. From the transmission spectrum shown in Figure 7b, we can see a transport gap of 1.65 eV and a hole SBH of 0.34 eV. From the local density of states plotted in Figure 7c, a band gap

of ~1.8 eV in the free ML WSe_2 region (dark blue) and a hole SBH of ~ 0.35 eV are clearly visible, comparable with the corresponding values derived from the transmission spectrum. The band bending of the free ML WSe_2 near the interface is not sharp, showing a weak built-in electric field between the source/drain and channel region. The SBH calculated in the transport simulation (0.34-0.35 eV) is consistent with that (0.34 eV) calculated from the energy band analysis without inclusion of the SOC.

This good agreement indicates that the energy band calculation is suitable in describing the vertical SBH in the weak and medium bonding contacts although it often gives an artificial vanishing lateral SBH in the strong bonding contacts.[24, 52] The reason lies in that in the vertical SBH calculation of a weak bonding contact, the coupling between the metal surface and the semiconductor is taken into account where the two parts are treated as a whole, but in the lateral SBH calculation of a strong bonding contact, the coupling between the source/drain region (metal and metal contacted 2D semiconductor) and the channel semiconductor is not considered where they are treated separately. Since WSe_2-Pt belongs to the medium bonding contact, we therefore believe that the Ohmic or quasi-Ohmic feature of ML/BL WSe_2-Pt contacts should be kept in a quantum transport simulation with inclusion of the SOC though it is unavailable now.

To provide a clear picture, the SBHs obtained by different methods are summarized in Figure 8. When contacted with the same metal, compared with those in ML case, the electron and hole SBHs in BL case both tend to be decreased due to the much reduced band gap. From left to right, the ML and BL WSe_2 are gradually changed from *n*- to *p*-type doping, which can be utilized to build *p*–*n* junctions, the most fundamental device building blocks for diverse optoelectronic functions. A ML WSe_2 device with Ti as cathode and Pd as anode is synthesized and can serve as a solar cell, photodiode, and light-emitting diode with impressive performances.[10] *P*-type ML WSe_2-Pd contact has a smaller SBH compared with Ag and Au contacts, which is well consistent with the contact resistance measurement.[5] In the absence of the SOC, Pd contact has the smallest hole SBH with a value no less than 0.22 eV though Pt has a larger work function than Pd (5.76 eV vs 5.36 eV in our work as given in Table 1). However, Pt contact wins the smallest hole SBH (actually 0 eV) in the presence of the SOC.

Note that the *p*-type WSe_2 FET in contact with metal Pt/Au/Pd electrode reported by Javey *et al.*[6] has a large contact resistance of about 1 Mohm•um, whereas another experiment confirms our prediction of the ohmic WSe_2-Pt contact.[65] The inconsistence in these two reports may result from the different fabrication processes and experimental conditions. In Ref. 6, a Pt/Au/Pd (10/30/20 nm)

metal stack is directly deposited on WSe_2 as a top-contact, whereas in Ref. 65, the WSe_2 is stamped onto the prepatterned Cr/Pt electrodes. There also exist some discrepancies between computational simulation and experimental results. Banerjee *et. al.* claimed that the contacts between ML MSe_2 and Ti, In, and Ag are *n*-type Ohmic in terms of their observed linear output characteristics.[4] However, in our opinion from the observed larger contact resistance and lower two-terminal field-effect mobility in the Ti contact compared with In and Ag contacts, the Ti contact appears not Ohmic. Nearly linear I_{ds}-V_{ds} characteristics in the low-voltage regime can be attributed to thermally assisted tunneling through a Schottky barrier at room temperature. The simulation study done by the same group revealed that Ti and In form *n*-type Schottky barriers to ML WSe_2 with heights of 0.33 and 0.47 eV, respectively.[21] And our calculations show that Ag forms a *n*-type Schottky contact to ML WSe_2. The reasons of these contradictive results may lie in that the TMD-metal interface is highly sensitive to the experimental processing environment such as vacuum conditions in the deposition chamber, deposition rate, and metal topography.

In the light of Schottky barrier and tunneling barrier, the nature of investigated ML WSe_2- metal contacts can be classified into four types as summarized in Figure 9. ML WSe_2-Sc contact is type I with a vanishing tunneling barrier and a finite *n*-type lateral Schottky barrier (Figure 9a). A non-zero tunneling barrier exists in the rest three types of contacts. Schottky barrier is formed at the interface B in type II (*n*-type) and III (*p*-type). The nature of ML WSe_2-Al, -Ag and -Au belongs to type II (Figure 9b) and that of ML WSe_2-Pd belongs to type III (Figure 9c). Type IV (ML WSe_2-Pt) can be expected as an excellent contact interface with an Ohmic or quasi-Ohmic contact (Figure 9d). However, the tunneling barrier with moderate tunneling probabilities (31.0% for Pt) would degrade its performance. As for BL WSe_2, BL WSe_2-Sc, Al, Ag, Pd and Pt interfaces keep the same contact type as the corresponding ML ones. However, WSe_2-Au changes into type III contact in BL case. It should be stressed that the band bending direction is opposite in 2D semiconductor-metal and the corresponding *n*- or *p*-type conventional bulk semiconductor-metal blocking contacts (Figure S5). The band of 2D semiconductors is bent upward in *p*-type contact[36] and bent downward in *n*-type contact when approaching the metal.

It has been pointed out that the actual transport gap of the channel, which could be descripted by the DFT band gap as a good approximation, equals to the quasi-particle band gap of heavily doped semiconductor. Therefore, a small correction to the DFT gap may be needed (an increase by about 10%).[54] An increase by about 10% in the band gap of ML/BL WSe_2 with the SOC effects implies a decrease and increase of about 0.06 eV in the VBM and CBM, respectively (half band gap

correction), and such a correction may lead to a small correction to the SBH (less than 0.06 eV in light of the Fermi level pining effect).

When different facets of metals contacted with the same 2D materials, the SBH may usually be different, because the different facets of metals reveal facet-dependent surface energies, surface states and work functions thus leading to different contact behaviors.[68] For example, the calculated hole SBH in the phosphorene-Ti (0001) contact is 0.30 eV, while in the phosphorene-Ti (1100) contact it is 0.57 eV.[52] Therefore, the SBH would change if WSe_2 contacts with other facet surfaces instead of (111) in fcc and (0001) in hcp metals studied in this work.

Conclusions

We provide the first comparative study of the interfacial properties of ML and BL WSe_2 on Sc, Al, Ag, Au, Pd, and Pt surfaces by using *ab initio* energy band calculations with inclusion of the SOC effects and a dual interface model. Compared with ML WSe_2-metal contacts, the electron and hole SBHs are decreased in BL WSe_2-metal contacts due to the smaller band gap in BL WSe_2, and the polarity of WSe_2-Au contact changes from *n*-type to *p*-type. The hole SBH is greatly reduced by the SOC effects in both ML and BL WSe_2-metal contacts. In the absence of the SOC, Pd contact has the smallest hole SBH with a value no less than 0.22 eV. Dramatically, *p*-type Ohmic or quasi-Ohmic contact appears in ML and BL WSe_2-Pt interfaces with inclusion of the SOC. *Ab initio* quantum transport simulation gives a similar SBH for ML WSe_2-Pt interface in the absence of the SOC. This fundamental study gives a deep insight into 2D WSe_2-metal interfaces and provides a theoretical foundation for the selection of metal electrodes in WSe_2 devices.

ASSOCIATED CONTENT

Supporting Information

Orbital-projected band structure and density of states of the ML WSe_2-Pt contact (Figure S1), band alignments between ML and BL WSe_2 and various metals (Figures S2 and S3), calculated Fermi level shift ΔE_f as a function of $W_M - W_{WSe2}$ (Figure S4), and illustrations of the band bending of 2D WSe_2-metal and conventional semiconductor-metal contacts (Figure S5). This material is available free of charge via the Internet at http://pubs.acs.org.

AUTHOR INFORMATION

Corresponding Author
*Tel: +86 10 62754105. Fax: +86 10 62751615. E-mail: jinglu@pku.edu.cn
Notes
The authors declare no competing financial interest.

ACKNOWLEDGMENTS

This work was supported by the National Natural Science Foundation of China (Nos. 11274016, 11474012, 11047018, and 60890193), the National Basic Research Program of China (Nos. 2013CB932604 and 2012CB619304), Fundamental Research Funds for the Central Universities, and National Foundation for Fostering Talents of Basic Science (No. J1030310/No. J1103205).

Notes and references

1. Q. H. Wang, K. Kalantar-Zadeh, A. Kis, J. N. Coleman and M. S. Strano, *Nature Nanotech.*, 2012, **7**, 699-712.
2. B. Radisavljevic, A. Radenovic, J. Brivio, V. Giacometti and A. Kis, *Nature Nanotech.*, 2011, **6**, 147-150.
3. S. Das, H.-Y. Chen, A. V. Penumatcha and J. Appenzeller, *Nano Lett.*, 2013, **13**, 100-105.
4. W. Liu, J. Kang, D. Sarkar, Y. Khatami, D. Jena and K. Banerjee, *Nano Lett.*, 2013, **13**, 1983-1990.
5. H. Fang, S. Chuang, T. C. Chang, K. Takei, T. Takahashi and A. Javey, *Nano Lett.*, 2012, **12**, 3788-3792.
6. M. Tosun, S. Chuang, H. Fang, A. B. Sachid, M. Hettick, Y. Lin, Y. Zeng and A. Javey, *ACS Nano*, 2014, **8**, 4948-4953.
7. N. Lu, H. Guo, L. Wang, X. Wu and X. C. Zeng, *Nanoscale*, 2014, **6**, 4566-4571.
8. W. Zhao, R. M. Ribeiro and G. Eda, *Acc. Chem. Res.*, 2014, **48**, 91-99.
9. J. S. Ross, P. Klement, A. M. Jones, N. J. Ghimire, J. Yan, D. G. Mandrus, T. Taniguchi, K. Watanabe, K. Kitamura, W. Yao, D. H. Cobden and X. Xu, *Nature Nanotech.*, 2014, **9**, 268-272.
10. A. Pospischil, M. M. Furchi and T. Mueller, *Nature Nanotech.*, 2014, **9**, 257-261.
11. N. Lu, H. Guo, L. Li, J. Dai, L. Wang, W.-N. Mei, X. Wu and X. C. Zeng, *Nanoscale*, 2014, **6**, 2879-2886.
12. A. T. Neal, H. Liu, J. Gu and P. D. Ye, *ACS Nano*, 2013, **7**, 7077-7082.
13. D. Xiao, G.-B. Liu, W. Feng, X. Xu and W. Yao, *Phys. Rev. Lett.*, 2012, **108**, 196802.
14. H. Yuan, M. S. Bahramy, K. Morimoto, S. Wu, K. Nomura, B.-J. Yang, H. Shimotani, R. Suzuki, M. Toh, C. Kloc, X. Xu, R. Arita, N. Nagaosa and Y. Iwasa, *Nature Phys.*, 2013, **9**, 563-569.
15. X. Xu, W. Yao, D. Xiao and T. F. Heinz, *Nature Phys.*, 2014, **10**, 343-350.
16. A. M. Jones, H. Yu, N. J. Ghimire, S. Wu, G. Aivazian, J. S. Ross, B. Zhao, J. Yan, D. G. Mandrus, D. Xiao, W. Yao and X. Xu, *Nature Nanotech.*, 2013, **8**, 634-638.
17. K. F. Mak, K. L. McGill, J. Park and P. L. McEuen, *Science*, 2014, **344**, 1489-1492.
18. C.-H. Lee, G.-H. Lee, A. M. van der Zande, W. Chen, Y. Li, M. Han, X. Cui, G. Arefe, C. Nuckolls, T. F. Heinz, J. Guo, J. Hone and P. Kim, *Nature Nanotech.*, 2014, **9**, 676-681.
19. E. J. Sie, J. W. McIver, Y.-H. Lee, L. Fu, J. Kong and N. Gedik, *Nature Mater.*, 2015, **14**, 290–294.
20. J. Kim, X. Hong, C. Jin, S.-F. Shi, C.-Y. S. Chang, M.-H. Chiu, L.-J. Li and F. Wang, *Science*, 2014, **346**, 1205-1208.
21. J. Kang, W. Liu, D. Sarkar, D. Jena and K. Banerjee, *Phys. Rev. X*, 2014, **4**, 031005.
22. J. Kang, S. Tongay, J. Zhou, J. Li and J. Wu, *Appl. Phys. Lett.*, 2013, **102**, 012111.
23. R. Cheng, D. Li, H. Zhou, C. Wang, A. Yin, S. Jiang, Y. Liu, Y. Chen, Y. Huang and X. Duan, *Nano Lett.*, 2014, **14**, 5590-5597.
24. H. Zhong, Z. Ni, Y. Wang, M. Ye, Z. Song, Y. Pan, R. Quhe, J. Yang, L. Yang, J. Shi and J. Lu, *arXiv:1501.01071 [cond-mat.mes-hall]*, 2015.
25. Y. Pan, Y. Wang, L. Wang, H. Zhong, R. Quhe, Z. Ni, M. Ye, W.-N. Mei, J. Shi, W. Guo, J. Yang and J. Lu, *Nanoscale*, 2015, **7**, 2116-2127.
26. C. Gong, L. Colombo, R. M. Wallace and K. Cho, *Nano Lett.*, 2014, **14**, 1714-1720.
27. J. Kang, W. Liu and K. Banerjee, *Appl. Phys. Lett.*, 2014, **104**, 093106.
28. W. Chen, E. J. G. Santos, W. Zhu, E. Kaxiras and Z. Zhang, *Nano Lett.*, 2013, **13**, 509-514.
29. I. Popov, G. Seifert and D. Tománek, *Phys. Rev. Lett.*, 2012, **108**, 156802.
30. L. Wei, K. Jiahao, C. Wei, D. Sarkar, Y. Khatami, D. Jena and K. Banerjee, IEEE International Electron Devices Meeting (IEDM), Washington DC, 2013.
31. S. Walia, S. Balendhran, Y. Wang, R. Ab Kadir, A. Sabirin Zoolfakar, P. Atkin, J. Zhen Ou, S. Sriram, K. Kalantar-zadeh and M. Bhaskaran, *Appl. Phys. Lett.*, 2013, **103**, 232105.
32. M. Amani, M. L. Chin, A. G. Birdwell, T. P. O'Regan, S. Najmaei, Z. Liu, P. M. Ajayan, J. Lou and M. Dubey, *Appl. Phys. Lett.*, 2013, **102**, 193107.
33. M. Farmanbar and G. Brocks, *Phys. Rev. B*, 2015, **91**, 161304.
34. W. S. Leong, X. Luo, Y. Li, K. H. Khoo, S. Y. Quek and J. T. L. Thong, *ACS Nano*, 2015, **9**, 869-877.
35. S. Chuang, C. Battaglia, A. Azcatl, S. McDonnell, J. S. Kang, X. Yin, M. Tosun, R. Kapadia, H. Fang, R. M. Wallace and A. Javey, *Nano Lett.*, 2014, **14**, 1337-1342.
36. S. McDonnell, A. Azcatl, R. Addou, C. Gong, C. Battaglia, S. Chuang, K. Cho, A. Javey and R. M. Wallace, *ACS Nano*, 2014, **8**, 6265-6272.
37. T. Musso, P. V. Kumar, A. S. Foster and J. C. Grossman, *ACS Nano*, 2014, **8**, 11432-11439.
38. W. S. Yun, S. W. Han, S. C. Hong, I. G. Kim and J. D. Lee, *Phys. Rev. B*, 2012, **85**, 033305.
39. S. J. Clark, M. D. Segall, C. J. Pickard, P. J. Hasnip, M. J. Probert, K. Refson and M. C. Payne, *Z. Kristallogr.*, 2005, **220**, 567-570.
40. D. Vanderbilt, *Phys. Rev. B*, 1990, **41**, 7892-7895.
41. F. Ortmann, F. Bechstedt and W. G. Schmidt, *Phys. Rev. B*, 2006, **73**, 205101.

42. P. E. Blochl, *Phys. Rev. B*, 1994, **50**, 17953-17979.
43. G. Kresse and D. Joubert, *Phys. Rev. B*, 1999, **59**, 1758-1775.
44. G. Kresse and J. Hafner, *Phys. Rev. B*, 1993, **47**, 558-561.
45. G. Kresse and J. Hafner, *Phys. Rev. B*, 1994, **49**, 14251-14269.
46. G. Kresse and J. Furthmuller, *Comput. Mater. Sci.*, 1996, **6**, 15-50.
47. G. Kresse and J. Furthmuller, *Phys. Rev. B*, 1996, **54**, 11169-11186.
48. H. J. Monkhorst and J. D. Pack, *Phys. Rev. B*, 1976, **13**, 5188-5192.
49. J. P. Perdew and Y. Wang, *Phys. Rev. B*, 1992, **45**, 13244-13249.
50. A. A. Al-Hilli and B. L. Evans, *J. Cryst. Growth*, 1972, **15**, 93-101.
51. Q. Liu, L. Li, Y. Li, Z. Gao, Z. Chen and J. Lu, *J. Phys. Chem. C*, 2012, **116**, 21556-21562.
52. Y. Pan, Y. Wang, M. Ye, R. Quhe, H. Zhong, Z. Song, X. Peng, J. Li, J. Yang, J. Shi and J. Lu, *arXiv:1507.02420 [cond-mat.mes-hall]*, 2015.
53. H. Qiu, L. Pan, Z. Yao, J. Li, Y. Shi and X. Wang, *Appl. Phys. Lett.*, 2012, **100**, 123104.
54. R. Quhe, R. Fei, Q. Liu, J. Zheng, H. Li, C. Xu, Z. Ni, Y. Wang, D. Yu, Z. Gao and J. Lu, *Sci. Rep.*, 2012, **2**, 853.
55. S. Das, W. Zhang, M. Demarteau, A. Hoffmann, M. Dubey and A. Roelofs, *Nano Lett.*, 2014, **14**, 5733-5739.
56. V. Tran, R. Soklaski, Y. Liang and L. Yang, *Phys. Rev. B*, 2014, **89**, 235319.
57. X. Wang, A. M. Jones, K. L. Seyler, V. Tran, Y. Jia, H. Zhao, H. Wang, L. Yang, X. Xu and F. Xia, *Nature Nanotech.*, 2015, **10**, 517-521.
58. J. Qiao, X. Kong, Z.-X. Hu, F. Yang and W. Ji, *Nature Commun.*, 2014, **5**, 4475.
59. H. Liu and N. A., *ACS Nano*, 2014, **8**, 4033–4041.
60. X. Peng, Q. Wei and A. Copple, *Phys. Rev. B*, 2014, **90**, 085402.
61. Y. Cai, G. Zhang and Y.-W. Zhang, *Sci. Rep.*, 2014, **4**, 6677.
62. J. Zheng, Y. Wang, L. Wang, R. Quhe, Z. Ni, W.-N. Mei, Z. Gao, D. Yu, J. Shi and J. Lu, *Sci. Rep.*, 2013, **3**, 2081.
63. V. Heine, *Phys. Rev.*, 1965, **138**, A1689-A1696.
64. H. Fang, M. Tosun, G. Seol, T. C. Chang, K. Takei, J. Guo and A. Javey, *Nano Lett.*, 2013, **13**, 1991-1995.
65. H. C. P. Movva, A. Rai, S. Kang, K. Kim, B. Fallahazad, T. Taniguchi, K. Watanabe, E. Tutuc and S. K. Banerjee, *ACS Nano*, 2015, **9**, 10402–10410.
66. G.-H. Lee, S. Kim, S.-H. Jhi and H.-J. Lee, *Nature Commun.*, 2015, **6**, 6181.
67. X. Ji, J. Zhang, Y. Wang, H. Qian and Z. Yu, *Phys. Chem. Chem. Phys.*, 2013, **15**, 17883-17886.
68. A. Michaelides and M. Scheffler, in *Textbook of Surface and Interface Science*, ed. K. Wandelt, Wiley-VCH 2010, vol. I

Table 1. Calculated interfacial properties of ML and BL WSe_2 on the metal surfaces. a_{hex}^{exp} represents the experimental cell parameters of the surface unit cells shown in Figure 1 for various metals, with lattice mismatch in percentage given below in parenthesis. The equilibrium distance d_z is the averaged distance between the surface Se atoms of WSe_2 and the relaxed positions of the topmost metal layer in the z direction. E_b is the binding energy per surface W atom between WSe_2 and a given metal. W_M and W are the calculated work functions for clean metal surface and WSe_2-metal contact, respectively. The SBHs obtained from band calculation with (without) inclusion of the SOC, transport simulation without inclusion of the SOC, and obtained in the previous work without inclusion of the SOC are given for comparison. Electron SBH is given for *n*-type Schottky barrier and hole SBH is given for *p*-type Schottky barrier. The Schottky barrier is always formed at the vertical direction except for Sc surface.

Metal	a_{hex}^{exp} (Å)	W_M (eV)	ML WSe_2				BL WSe_2			
			d_z (Å)	E_b (eV)	W (eV)	SBH (eV)	d_z (Å)	E_b (eV)	W (eV)	SBH (eV)
Sc	3.308 (0.55%)	3.60	2.736	0.918	3.75	0.29^{n} $(0.25^{n})^{S}$	2.512	1.049	3.94	0.16^{n} $(0.25^{n})^{S}$
Al	5.720 (0.38%)	4.12	2.959	0.288	4.15	0.70^{n}	2.885	0.367	4.16	0.37^{n}
Ag	5.778 (1.40%)	4.49	2.693	0.302	4.26	0.50^{n}	2.684	0.240	4.56	0.30^{n}
Au	5.768 (1.22%)	5.23	2.712	0.182	4.71	0.66^{n} $(0.70^{n})^{a}$	2.773	0.160	4.85	0.58^{p}
Pd	5.500 (3.48%)	5.36	2.395	0.602	4.84	0.22^{p} $(0.35^{p})^{a}$ $(0.23^{p})^{S}$	2.271	0.706	5.05	0.27^{p} $(0.09^{p})^{S}$
Pt	5.549 (2.70%)	5.76	2.652	0.525	5.22	0.34^{p} $(0.34^{p})^{T}$ $(0.00^{p})^{S}$	2.770	0.597	5.21	0.32^{p} $(0.00^{p})^{S}$

[a] From Ref. [21].
[n] *n*-type Schottky barrier.
[p] *p*-type Schottky barrier.
[S] In the presence of the SOC.
[T] Value from the transport simulation.

Table 2. Tunneling barrier height ΔV, width w_B, and probabilities (T_B) through the ML/BL WSe_2.

Metal	ML WSe_2			BL WSe_2		
	ΔV (eV)	w_B (Å)	T_B (%)	ΔV (eV)	w_B (Å)	T_B (%)
Sc	0.000	0.000	100	0.000	0.000	100
Al	2.284	0.850	26.9	0.996	0.720	47.9
Ag	1.787	0.670	39.9	0.87	0.68	52.2
Au	2.199	0.704	34.3	1.282	0.734	42.7
Pd	1.477	0.518	52.4	0.555	0.313	78.8
Pt	2.533	0.716	31.0	1.420	0.731	41.0

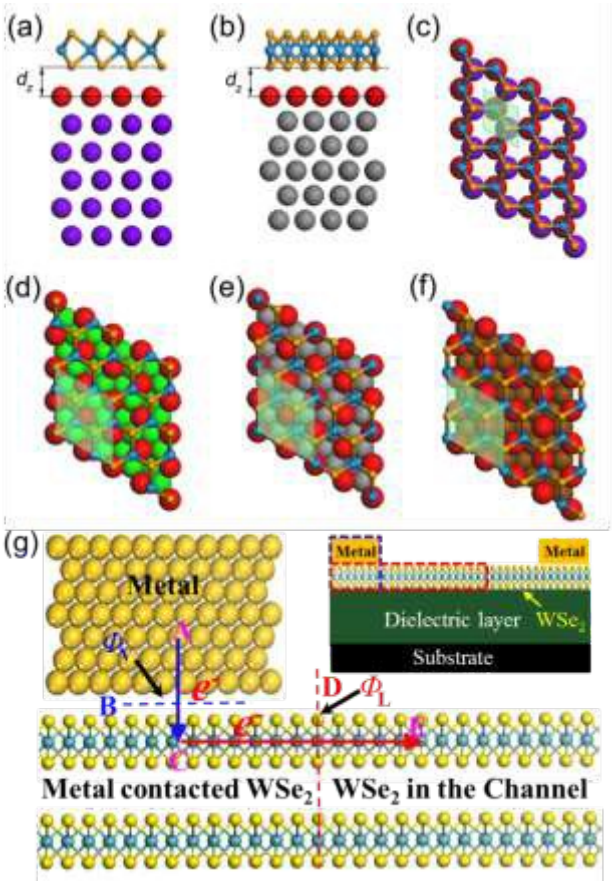

Figure 1. Interfacial structures of the most stable configuration for ML WSe_2 on metal surfaces. Side views of (a) WSe_2 on Sc(0001) surface and (b) on other metal surfaces. Top views of contacts (c) Sc-WSe_2, (d) Al/Pt-WSe_2, (e) Pd-WSe_2, (f) Ag/Au-WSe_2. d_z is the equilibrium distance between the metal surface and the bottom layer WSe_2. The rhombi plotted in light green shadow shows the unit cell for each structure. (g) Schematic cross-sectional view of a typical metal contact to intrinsic WSe_2. A, C, and E denote the three regions while B and D are the two interfaces separating them. Blue and red arrows show the pathway (A→B→C→D→E) of electron injection from contact metal (A) to the WSe_2 channel (E). Inset figure shows the typical topology of a WSe_2 field effect transistor.

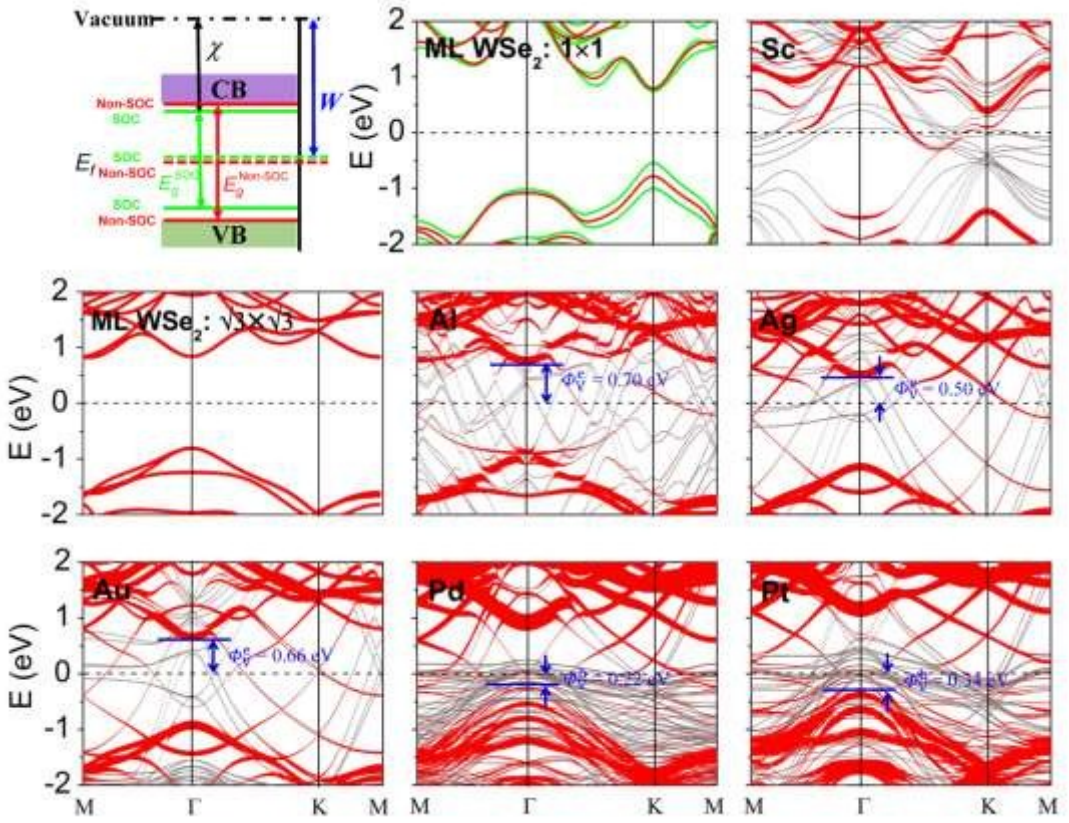

Figure 2. First panel: Schematic illustration of the absolute band positions with respect to the vacuum level by the DFT method with and without inclusion of the SOC effects for ML WSe_2. The rest: Band structures of ML WSe_2 and ML WSe_2-Sc, -Al, -Ag, -Au, -Pt, and -Pt contacts, respectively. Gray line: metal surface bands; red line: bands of WSe_2 without considering the SOC effects. The line width is proportional to the weight. Green line: bands of WSe_2 with the SOC effects. The Fermi level is set at zero.

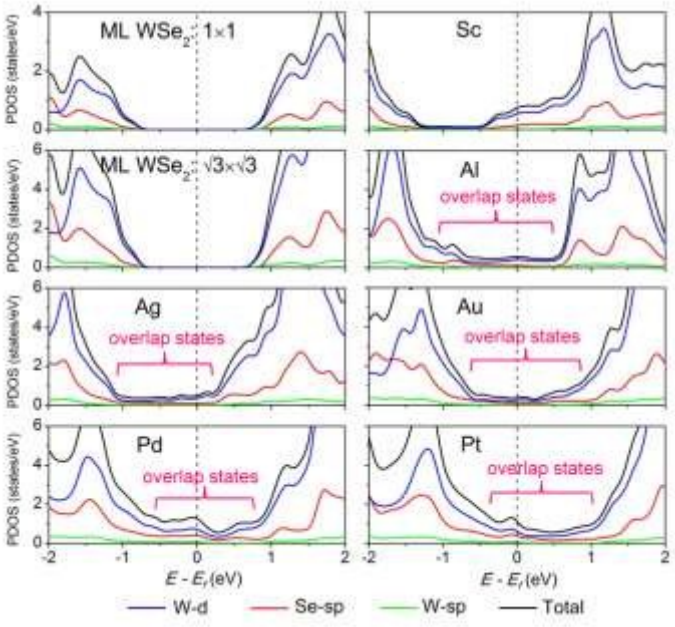

Figure 3. Partial density of states (PDOS) of W and Se electron orbitals, for ML WSe_2, ML WSe_2-Sc, -Al, -Ag, -Au, -Pd, and -Pt systems, respectively, in the absence of the SOC. The blue, red, green, and black curves represent *d*-orbital of W atoms, *sp*-orbital of Se atoms, *sp*-orbital of W atoms, and the total PDOS as indicated by the legend below the plot. The Fermi level is set at zero.

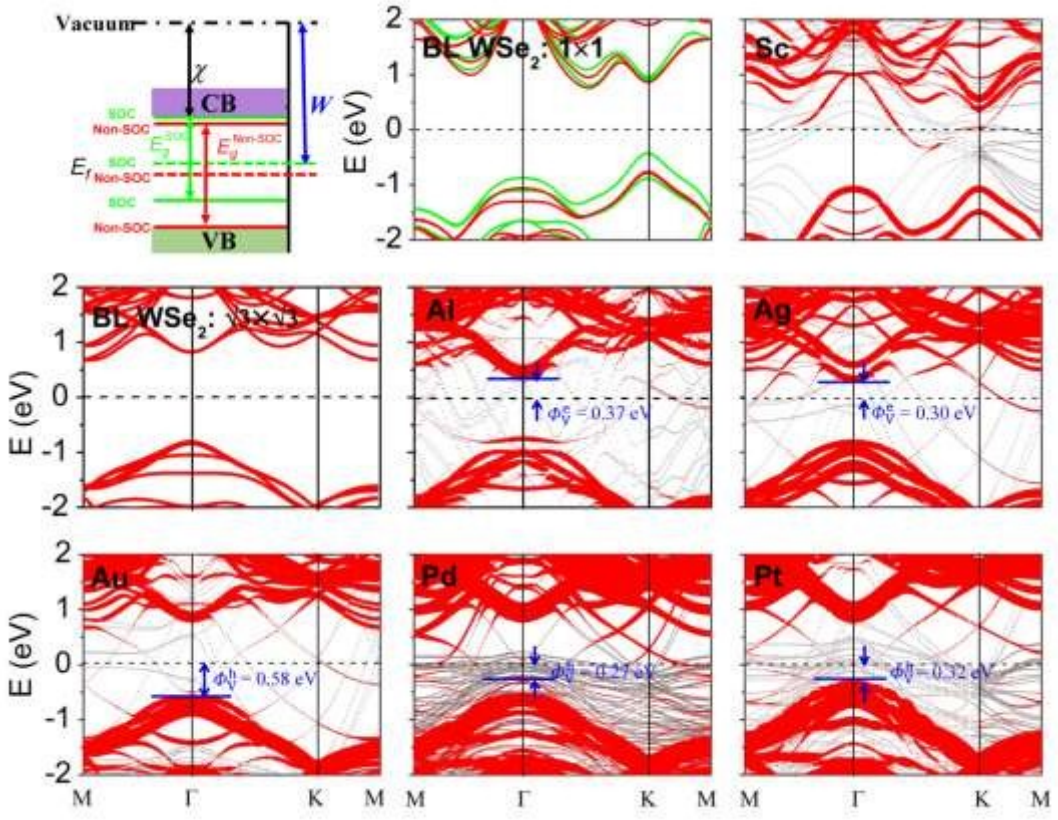

Figure 4. First panel: Schematic illustration of the absolute band positions with respect to the vacuum level by the DFT method with and without inclusion of SOC effects for BL WSe_2. The rest: Band structures of BL WSe_2 and BL WSe_2-Sc, -Al, -Ag, -Au, -Pt, and -Pt contacts, respectively. Gray line: metal surface bands; red line: bands of WSe_2 without considering the SOC effects. The line width is proportional to the weight. Green line: bands of WSe_2 with the SOC effects. The Fermi level is set at zero.

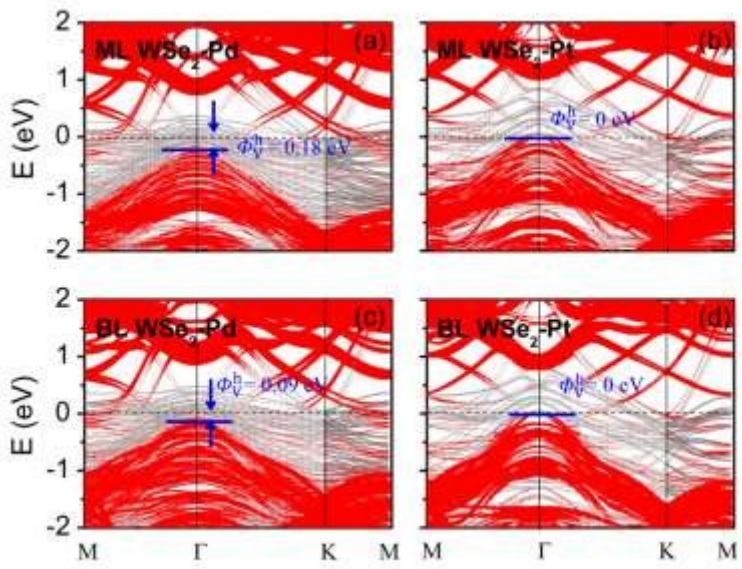

Figure 5. Band structures of (a,b) ML and (c,d) BL WSe_2 on (a,c) Pd, and (b,d) Pt surfaces with the SOC effects, respectively. Gray line: metal surface bands; red line: bands of WSe_2. The line width is proportional to the weight. The Fermi level is set at zero.

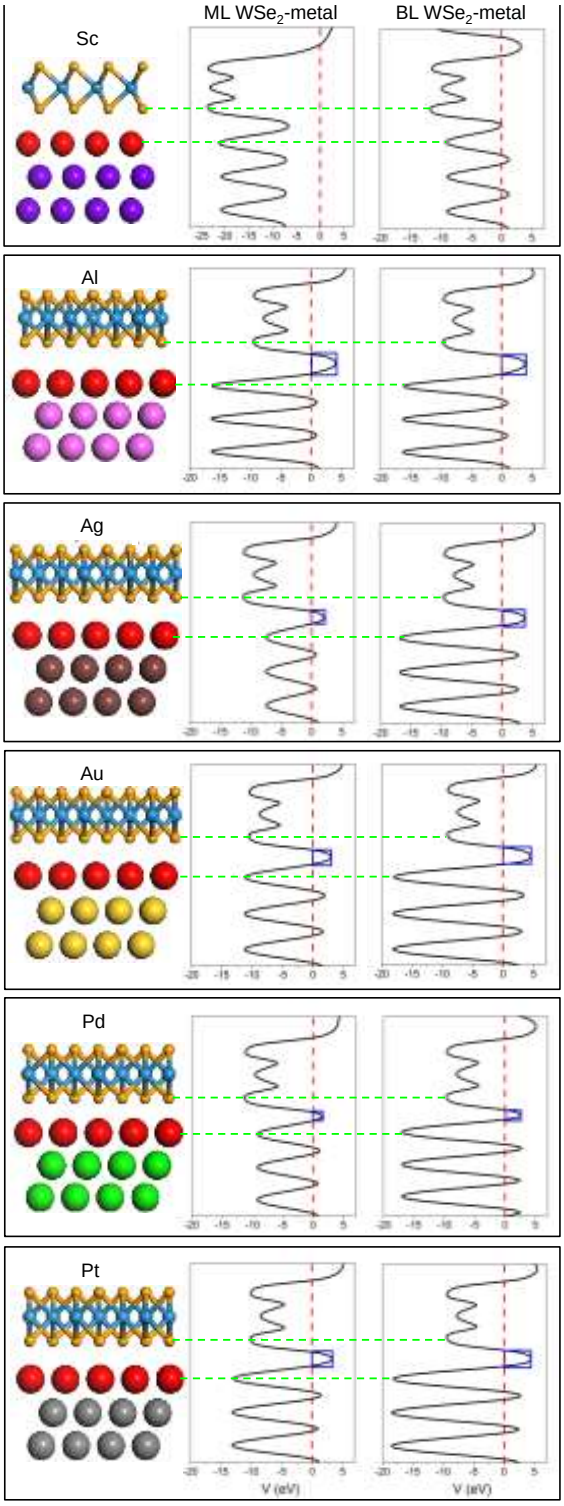

Figure 6. Average electrostatic potential *V* in planes normal to the ML and BL WSe_2-metal contacts. The red dash lines represent the Fermi level.

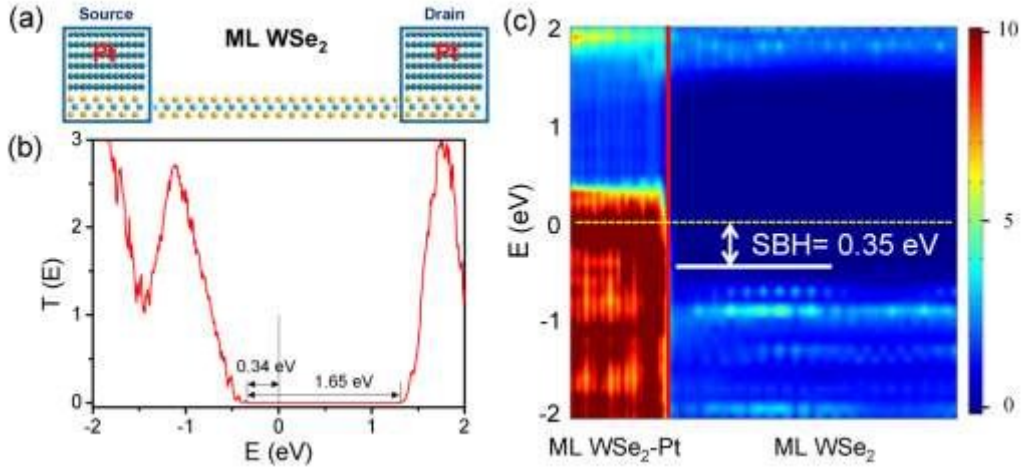

Figure 7. Simulation of a ML WSe_2 transistor with Pt as electrodes without inclusion of the SOC. (a) Schematic configuration. (b) Zero-bias transmission spectrum. The transport gap and hole SBH are indicated. (c) Local density of states (LDOS) in color coding for the device. The red line indicates the boundary of ML WSe_2/Pt and the free-standing ML WSe_2, and the yellow dashed line indicates the Fermi level.

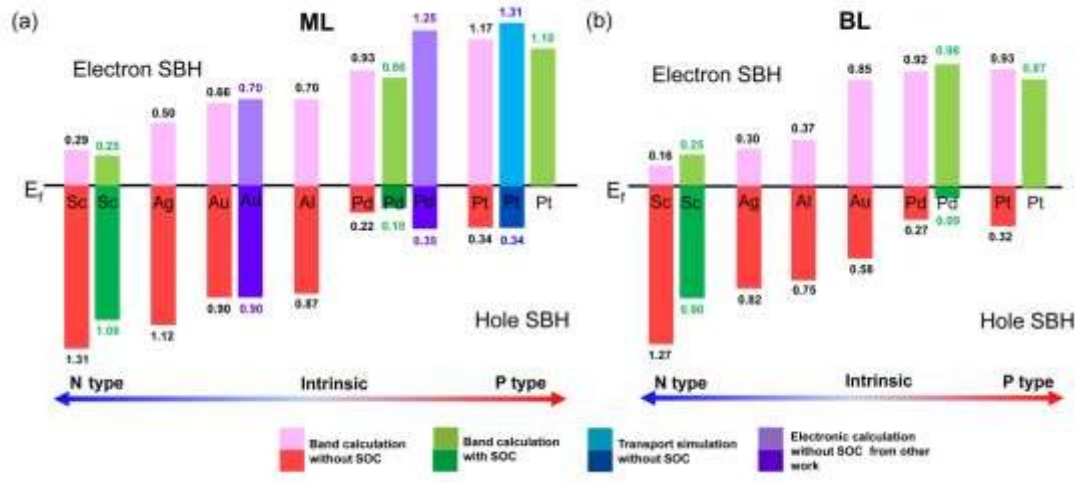

Figure 8. Electron and hole SBHs of (a) ML and (b) BL WSe_2-Sc, Al, Ag, Au, Pd and Pt contacts. The light (deep) red, green, blue, and purple rectangle present the electron (hole) SBH obtained from band calculation without the SOC, band calculation with the SOC, transport simulation without the SOC, and data from Ref. [21], respectively.

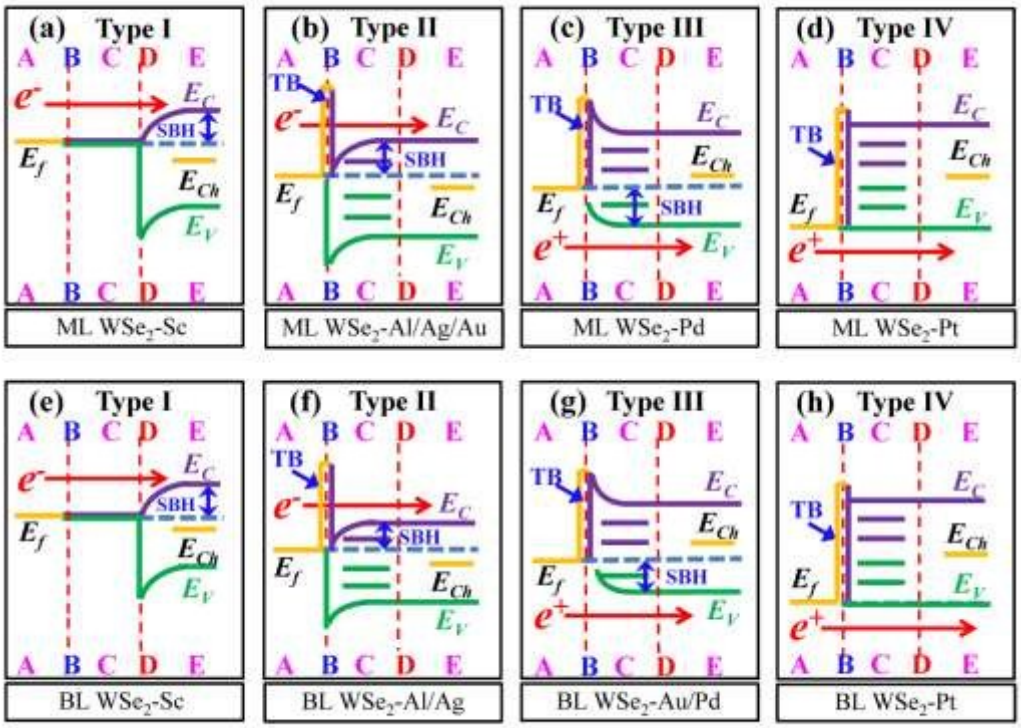

Figure 9. (a)-(h) Eight band diagrams of Figure 1(g), depending on the type of metals and WSe_2 layer number. Examples are provided at the bottom of each diagram. A~E represent the different regions or interfaces depicted in Figure 1(g). TB denotes the tunneling barrier at the interface B. E_f and E_{Ch} denote the Fermi level of the absorbed system and intrinsic channel WSe_2, respectively. E_c and E_v are the CBM and VBM of WSe_2, respectively. Red arrows indicate the direction of electron or hole flow.

TOC:

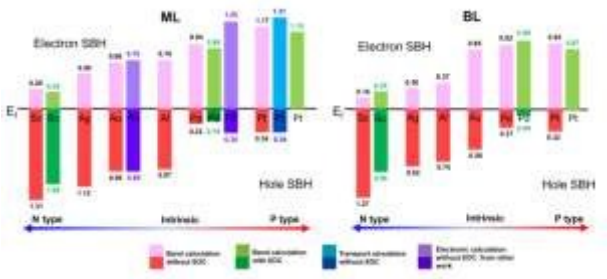

P-type Ohmic or quasi-Ohmic contact appears in ML and BL WSe_2-Pt interfaces with inclusion of the spin-orbital coupling.